

A Cloud-based Bi-directional LSTM Approach to Grid-connected Solar PV Energy Forecasting for Multi-Energy Systems

Qi Liu ^{#a}, Oscar Famous Darteh ^{#b}, Muhammad Bilal^{*c}, Xianming Huang^d, Muhammad Attique^{*e}, Xiaodong Liu^e and Amevi Acakpovi^g

^aWuxi University, No.333, Xishan Road, 214106, Jiangsu, China

^bSchool of Electronic and Communication Engineering, Nanjing University of Information Science and Technology, No.219, Ningliu Road, 210044, Jiangsu, China

^cDepartment of Computer and Electronics Systems Engineering, Hankuk University of Foreign Studies, Gyeonggi-do, 17035, Gyeonggi-do, Republic of Korea

^dSchool of Computer Science, Hunan University of Technology, Zhuzhou, 412007, Hunan, China

^eDepartment of Software, Sejong University, 05006 209, Seoul, Republic of Korea

^fSchool of Computing, Napier University, 10 Colinton Road, EH10 5DT, Edinburgh, UK

^gDept. of Electrical and Electronic Engineering, Accra Technical University, P.O.Box GP561, Accra, Barnes Road, Greater Accra, Ghana

ARTICLE INFO

Keywords:

Bi-directional LSTM
Solar Energy
Photovoltaic Forecasting
Grid-connected PV System
Multi-Energy Systems

ABSTRACT

The drive for smarter, greener, and more livable cities has led to research towards more effective solar energy forecasting techniques and their integration into traditional power systems. However, the availability of real-time data, data storage, and monitoring has become challenging. This research investigates a method based on Bi-directional LSTM (BDLSTM) neural network. BDLSTM takes into account the data's past and future context. The future hidden layer takes input in ascending order while the past hidden layer evaluates the input in decreasing order, making BDLSTM relevant in analyzing the input data's past context and evaluating future predictions. The eleven-year (2010-2020) weather dataset used for this paper was acquired from NASA. Two *pre-processing* approaches, Automatic Time Series Decomposition (ATSD) and Pearson correlation, were used to remove the noisy values from the residual components and for feature selection, respectively. To ensure storage and reuse of data, the architecture includes a cloud-based server for data management and reuse for future predictions. Popular in multi-energy systems, the cloud-based server also serves as a platform for monitoring predicted solar energy data. The metrics values and results obtained have demonstrated that the BDLSTM performs efficiently on the available data. Data from two separate climatic horizons proved the study's quality and reliability.

1. Introduction

Energy security is a critical problem, with solar energy being seen as one of the most promising means of achieving sustainable development, multi-energy systems and energy security (Liu, Kamoto and Liu (2020a)). Climate change, global warming, and rising energy needs have prompted governments worldwide to find ways to integrate cost-effective and ecologically friendly energy sources into the traditional grid (Hunter, Vettorato and Sagoe (2018)). The variability of solar energy is one of the most important challenges limiting the use of the source. Solar Energy is highly unpredictable; therefore, it is sometimes referred to as an unreliable energy source. Additionally, increases in the risk and uncertainty of generating the predicted solar energy impede energy security (Sindhu, Nehra and Luthra (2017)) since moving towards renewable energy have become critical.

Accurate forecasting and thorough solar energy analysis may assist decrease risk and enable assets to be operated

* Corresponding author: mbilal@hufs.ac.kr (Muhammad Bilal), attique@sejong.ac.kr (M. Attique)

Both authors have equal contribution as first author.

✉ qi.liu@nuist.edu.cn (Q.L. #); dartfamous@gmail.com (O.F.D. #); mbilal@hufs.ac.kr (M. Bilal*); huangxianming@hut.edu.cn (X. Huang); attique@sejong.ac.kr (M. Attique*); x.liu@napier.ac.uk (X. Liu); acakpovia@gmail.com (A. Acakpovi)

ORCID(s):

at the lowest possible cost. Solar energy may be planned, and accurate solar energy forecasts boost its penetration in multi-energy system planning. Solar energy prediction would provide early notice on power instability, allow optimum awareness for utility, and inform economic decisions. For this reason, it must be emphasized that the predictive model's accuracy is determined by the importance of the variables chosen for the prediction and the forecasting horizon in terms of the available data. Solar energy forecasts can range from very short-term to long-term, depending on compatibility.

Notwithstanding, predicting solar energy is not an easy task due to several factors, such as uncertainty of load demand (Na, Wang, Li, Xia, Liu, Xiong and Lu (2018)), load management (Zhang, Liu, Chen, Tian and Wang (2021)) and load monitoring (Liu, Kamoto, Liu, Zhang, Yang, Khosravi, Xu and Qi (2020b))-(Liu, Nakoty, Wu, Anaadumba, Liu, Zhang and Qi (2020c)), weather conditions, geographic locations, nature of data (Xu, Wang, Wang, Zhang and Hu (2021)), (Shen, Xu, Qi, Zhang and Srivastava (2021)) and seasons (Hu, Xu, Zhang, Tang, Cheng, Qian and Khosravi (2021)), especially in the emergence of multi-energy systems applications (Wu, Liu, Liu, Zhang and Yang (2022)) and maintenance (Darteh, Liu, Oduro, Liu and Adjei

(2021)). To ensure the reliability of solar energy, multi-energy system planners, for example, should routinely be informed of the phenomenon in forecasting research to aid energy management. Using unique and customized data coupled with an integrated solution is required to reduce errors and enable effective decision-making based on predictions created by reliable models.

Machine and deep learning techniques such as recurrent neural network (RNN) (Li, Wang, Zhang, Xin and Liu (2019)), long short term memory (LSTM) (Harrou, Kadri and Sun (2020)), gated recurrent unit (GRU) (Wang, Liao and Chang (2018a)), and multilayer perceptron (MLP) (El Badaoui, Abdallaoui and Chabaa (2013)) were used extensively for solar energy prediction. However, the main challenge with these models is the lack of rigorous data cleanings like ATSD, non-bidirectionality and the inability to propose a storage medium for the input and the predicted data. One of the challenge that affects the operation and management of solar energy in multi-energy systems is the volatile nature of solar energy generation due to unpredictable weather conditions. *Because operational management's role of instituting administrative functions that ensure energy dependability and market competitiveness, as well as power quality control, output control, and costs control, and proposes initiatives to mitigate environmental impacts in the energy business and multi-energy system initiatives*, this study presents a BDLSTM model combined with cloud-based Photovoltaic (PV) data management based on critical meteorological factors for 1 hour ahead of solar energy forecasting. *Also, BDLSTM has not been used in any recently solar energy prediction papers. Against this backdrop, this paper explores the BDLSTM solar energy forecasting approach coupled with data storage.* The following are this study's main contributions and goals:

- Automatic time-series decomposition is used smoothing meteorological variables to find the essential meteorological data, from which the model should learn to improve the accuracy;
- Various criteria and evaluation metrics are manipulated to assess the efficiency of the proposed BDLSTM for solar energy prediction;
- A cloud-based architecture has been implemented to store and process collected data for energy monitoring, control and future prediction.

The rest of this paper is organized as follows: Section 2, the most recent significant works in the solar energy forecasting field and research are done with BDLSTM. Section 3 covers the proposed cloud-based grid-connected PV System, Cloud-based data management, data gathering, data preprocessing, including automatic time series decomposition and Pearson correlation, and the description of the relevance of the proposed BDLSTM model in analyzing the past context of input data and evaluation of any future predictions. Section 4 covers experimental results and discussions, including

elaborating on the findings, and Section 5 summarizes the paper's content.

2. Related Work

This section discusses the most recent significant works in solar energy forecasting and other literature using the BDLSTM model. Literature on BDLSTM is exploratory. BDLSTM involves duplicating the recurrent layer in the network so that there are two layers side by side, then feeding the input sequence to the first layer and feeding a reversed duplicate of the input sequence to the second (Bansal, Sharma and Singh (2019)). BDLSTM has been instrumental in classification tasks such internet traffic intrusion detection (Ran, Zheng, Lai and Tian (2020)), network-wide traffic state with missing values (Cui, Ke, Pu and Wang (2020)), image captioning (Cao, Yang, Sun, Liang, Yang and Guan (2019a)) and user reference captioning (Zhao, You, Wen and Li (2020)). BDLSTM has also gained prominence in real-time monitoring and analyzing anomalous data in hydraulic systems (Kim and Jeong (2020)), early forest fire recognition based on features from videos (Cao, Yang, Tang and Lu (2019b)), and processing speech recognition (Yang, Li, Wang and Tang (2019)). Due to its tendency to split the state of the LSTM neurons in positive time directions (forward states) and negative time directions (reverse states), BDLSTM has become famous for predictive works in wireless sensor networks (Cheng, Zheng, Wang, Yang and Wan (2019)), wind speed prediction (Saeed, Li, Danish, Saeed, Tang, Gan and Ahmed (2020)), and multi-energy systems interactive motion prediction of cut-in vehicles in urban environments (Jeong and Yi (2020)). Despite the fact that it is powerful for forecasting models, BDLSTM is rarely used in the field of solar energy forecasting. Apart from statistical models such as auto-regressive with exogenous input, autoregressive moving average (ARMA) (Benmouiza and Cheknane (2016)) and autoregressive integrated moving average (ARIMA) (Agada, Eweh and Aondoakaa (2021)), machine learning has become popular these days in solar energy prediction (Mohanty, Patra and Sahoo (2015)). Over the years, machine learning and deep learning techniques for predicting solar energy have been proposed (Maciel, Ledesma and Junior (2021)), (Qing and Niu (2018)), (Sun, Wang, Zhang and Zheng (2018)), (Abualigah, Zitar, Almotairi, Hussein, Abd Elaziz, Nikoo and Gandomi (2022)). The most recently used solar energy forecasting models are GAM-based PV forecasting Choi and Hur (2020), Matsumoto and Yamada (2021) and Mpfumali et al.'s Convex and Quantile regression averaging (QRA) predictor work cited by Ilunga (2018). Research in McCandless, Dettling and Haupt (2020), Hmamouche, Przymus, Casali and Lakhali (2017) and Pasion, Wagner, Koschnick, Schuldt, Williams and Hallinan (2020), also deployed hyper-parameter tuning methods. Enhanced random forest (ERF) with Local Interpretable Model-Agnostic Explanations, Extreme Boosting Model, and Elastic Net as the feature selection strategies

in Massaoudi, Chihi, Sidhom, Trabelsi, Refaat and Oueslati (2021), Multilayer perceptron with grey wolf optimizer (MLP-GWO) and hybrid adaptive network-based fuzzy inference systems (ANFIS) in Claywell, Nadai, Felde, Ardabili and Mosavi (2020) with results evaluated using mean absolute error (MAE), mean square error (MSE), and root mean square error (RMSE). Regularized online sequential extreme learning machine integrated with variable forgetting factor (FOS-ELM) to predict global solar radiation at Bur Dedougou in Burkina Faso using Bayesian information criterion (BIC) to build the weather parameters was proposed in Hou, Zhang, Weng, Ali, Al-Ansari and Yaseen (2018). Authors, Kim, Jung and Sim (2019) employed a random forest regression (RFR) to predict solar power generation, achieving an R-squared value of 70.5 per cent in the test set. For precise short-term prediction of solar intensity based on meteorological data, a novel least absolute shrinkage and selection operator (LASSO) by Wang, Shen, Mao, Chen and Zou (2018b) and long short-term memory (LSTM) integrated forecasting model. It combines a fundamental time series model, data clustering, a statistical model, and machine learning into one system. All of the scientific contributions described above are fascinating. However, they do not offer a cloud-based solution for PV data management in multi-energy systems environments, except for the authors, Jebli, Belouadha, Kabbaj and Tilioua (2021) whose framework deals with temperature, solar radiation, energy, humidity, wind speed, direction, and pressure. Furthermore, the authors used only Pearson correlation as a feature selection tool, but our study also seeks to use automatic time series decomposition.

3. The Proposed Cloud-based Grid-connected PV System

This section describes the cloud-based grid-connected PV System, the forecasting architecture, data preprocessing, feature selection, and the architecture of the forecasting models.

3.1. A Cloud-based Grid-connected PV System

A cloud-based grid-connected PV system is the architecture under consideration for this work. A basic grid-connected PV system consists of a PV module, grid-connected inverters, and grid interface control. Circuit breakers and other hardware components make up the grid interface control. *The circuit breaker protects the system from over-currents due to grid overloads and short circuits. The grid-connected Inverter transforms direct current (DC) into alternating current (AC) appropriate for injection into the grid or consumption by the load, ensuring the anti-independence of the entire system, which is one of the goals of multi-energy systems.* The incorporated cloud-based server is shown in the architecture in Figure 1 is an internet-based server, whereby on-demand hardware and software resources are provided to users for data management. It is a by-product and consequence of the ease of access to remote computing

sites provided by the internet. *Since we do not have access to the hardware cloud server due to the expensive cost of acquiring data storage servers and the security concerns of using public servers, the google collaboratory environment is used. The google collaboratory gives affordable access to a graphics processing unit (GPU) that allows high data throughput and fast vector computation. The cloud GPU comes with 32GB boot RAM, and the boot RAM is used to store downloaded datasets for pre-processing as well as model input and output data.* Once the pre-processing described in subsection 4 is completed, pre-processed data is stored on the server. A user interface for data management is provided via a link. Forecasting models perform forecasting and evaluation directly from the drive and values stored on the drive for future forecasting. Since grid-connected inverters are equipped with PA300 to detect the power status at both grid and the PV side, recent grid networks have inbuilt Modbus communication protocol for two-way communication between the NetMeter and the Inverter cited in Swales et al. (1999). *The Modbus is a request-response protocol implemented using a master-slave relationship. In the master-slave relationship, communication always occurs in pairs, thus one device initiates a request the waits for a response and the initiating device (the Inverter) is responsible for initiating any interaction responsible with the net-meter either read production from the solar system or the grid.* Hence, a cloud server with an IP address can be ported. Meteorological factors such as solar irradiation, temperature, humidity, wind speed, and pressure are other factors that influence the energy production of solar energy, but in most cases, emphasis is laid on solar irradiation. Solar energy production can be established by computing the meteorological parameters suggested by AISkaif, Dev, Visser, Hossari and van Sark (2020). The solar energy generated at the output of a PV system is given by:

$$e_{PVout} = A * r * PR * H * t \quad (1)$$

where e_{PVout} is the energy in Wh , A is the total PV generator area in m^2 , r is the PV module efficiency, which is the ratio of the electrical power output of one PV to the cross-sectional area of one PV, given by:

$$r = P_{1PVout} / A_{1PV} \quad (2)$$

PR is the performance ratio, H is the solar irradiance at any time step falling on the surface of the solar PV module in watt-hour per squared meter (Wh/m^2) and t is the time at which data is taken in h . The performance ratio is a location-independent measure of a PV plant's quality, sometimes referred to as a quality factor by Rajasegarar, Leckie, Palaniswami and Bezdek (2007). Inverter losses, temperature losses, DC cable losses, AC cable losses, shadings, weak radiation, dust, snow, dew, and others are variables in the PR value. *The PV system's DC power is transferred through the DC cable. The issue with DC power is that it cannot be used directly by most appliances and gadgets but can be converted into AC power with the help of an inverter. Losses from DC and AC cable runs occur during*

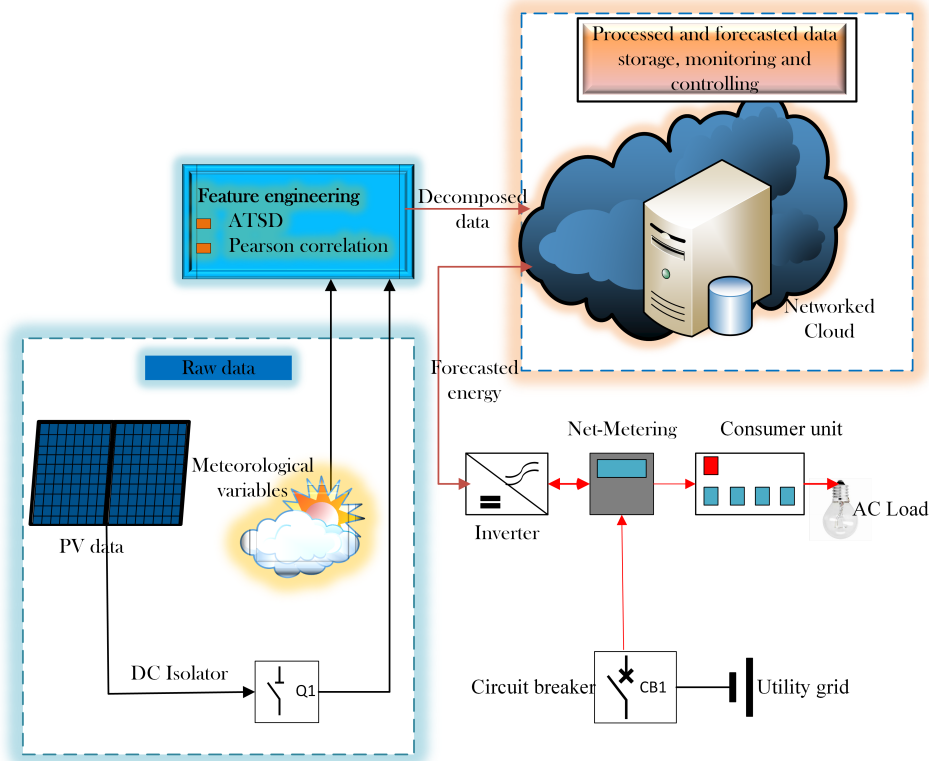


Figure 1: Cloud-based grid-connected PV system

Table 1

Parameters of the Test Bench PV module

Parameter	Symbol	Values
Maximum Power	P_{pvout}	575Wp
Maximum Power Voltage	V_{mp}	44.67v
Maximum Power Current	I_{mp}	12.88A
Operating Efficiency	r	21.30
Area of Unit PV module	A_{1PV}	2.734m ²

the design and installation stages due to the cable size and the cable runs' distance, insulation, and termination at devices. A default PR value of 0.75 is chosen where these variables are unknown (Solar and Ag (2016)). Because of its strong performance, PV module used to compute the solar energy is 3479 pieces of 575Wp Jinko TR Bifacial in Chen, Baek, Hou, Aydin, De Bastiani, Scheffel, Proppe, Huang, Wei, Wang et al. (2020) which gives approximate 2001kWp power output with parameters shown in Table 1.

3.2. The Forecasting architecture

The proposed forecasting architecture comprises five main processes, as shown in Figure 2 data collecting, data *pre-processing* (data filtering, handling missing data, data scaling, feature engineering, data splitting), algorithm training, and algorithm testing to analyze the model's performance. This architecture processes the meteorological dataset as variables and solar energy as the label. It should be noted that the architecture is employed for data in the

instance of Tamale in Ghana's Northern region. However, for the method's reliability, Wuhan, China, with a parallel climatic condition (Ye, Chen and Hou (2015)) is chosen as an additional test case. *The two climatic locations were selected due to the parallel variability in climatic conditions. For instance, according to World Weather Information (Ritterbush (2006)), Tamale's average annual sun hours is 2755, almost 1.5 times the average annual sun hours of 1870 in Wuhan. The average annual precipitation days in Tamale and Wuhan are 70 and 116, respectively. The eleven-year data (in time-steps of one hour from (2010-01-01,00 hours to 2020-12-31, 23 hours consisting of solar radiation, humidity, wind speed, UVA irradiance, and UBA irradiance was downloaded from POWER (2018). The UVA irradiance and UBA for solar energy prediction is important because they are almost constant up at 60 degrees and fall within the acceptable wavelength of 280-320 (UBA) and 320-400 (UVA). Even though UVA has not been considered harmful for years, research by Sola and Lorente (2015) recognizes its role in some biological response cases. Since we aim to predict solar energy, it is imperative to compute it using equation (1). The raw data used to train and test the BDLSTM are the variables, and the computed solar energy is the label. The web-based Jupyter notebook environment was used for simulation. The distribution of solar energy data for both geographical regions and the variance of solar energy on a particular day across the period were analyzed. In Tamale, for example, generation begins around 6 am, peaks at 12noon, and then gradually drops until it returns to zero*

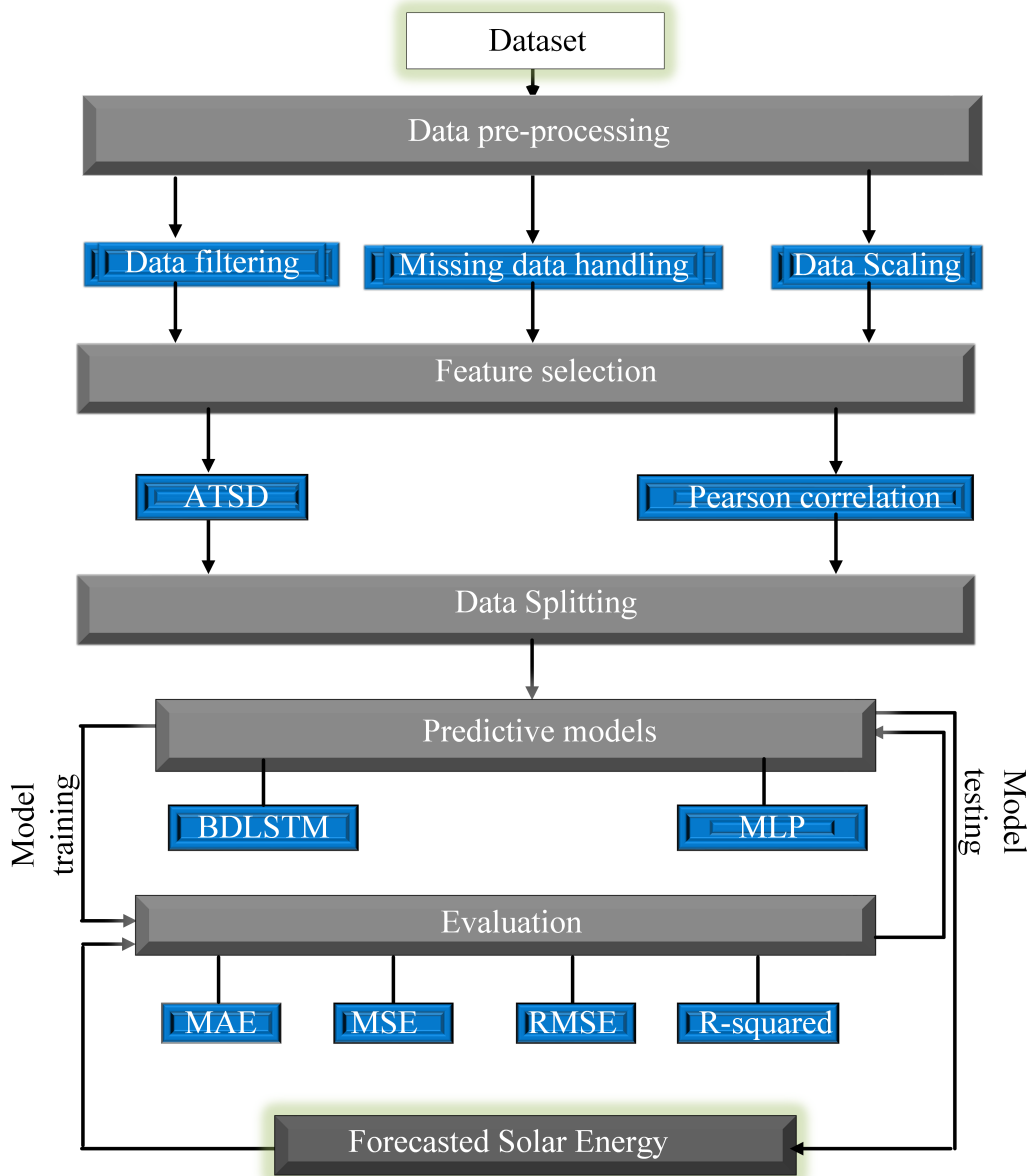


Figure 2: Proposed forecasting architecture.

at 6 pm. The hourly solar energy production trend appears crucial in a day, but it does not completely address the influence of seasonality owing to the geographic location's climatic circumstances. *This is because the hourly recorded irradiance is transient during the day and could not the seasonality.* As a result, the data were resampled in 24-hour, 168-hour, and 720-hour rolling windows, representing daily, weekly, and monthly, and the mean of each window was calculated. Because the data appears too dense, the daily window, like the hourly window for the time, shows no identifiable seasonality.

Overall, the weekly window appears the best, as illustrated in Figure 3, and the monthly window displays close uniform peaks and troughs, indicating some seasonality but shielding some noisy areas. For example, as shown in Figure 4, the amplitude of the maximum yearly variation in

proportion to the value common to the months changes every month. From 1 January to 31 December, the extreme value of energy swings between 25000 and 3000MWh. Although Tamale is in the dry season, poor solar energy output occurs between November and February due to the harmattan haze season. *Harmattan haze is defined by cold, dry, dust-laden wind and considerable temperature differences between day and night (Minka, Ayo et al. (2014)). Thick dust in the air significantly reduces solar irradiation.* We also discovered that the unstable trough witnessed between May and June was caused by precipitation in both regions. However, it is necessary to keep in mind that the showers do not occur during the entire month or day, which has also called into doubt the true impact of monthly seasonality on the data. In light of this, we aim to use the feature engineering approach in the next section.

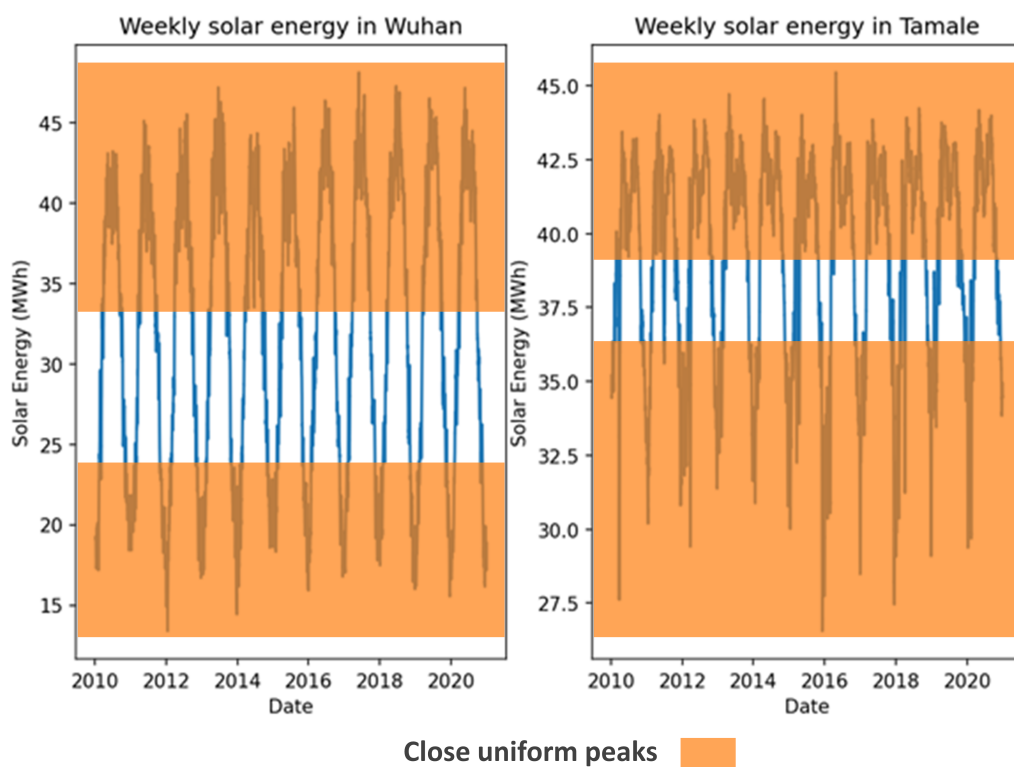


Figure 3: Weekly distribution of solar energy over the period studied (Tamale, left and Wuhan, right).

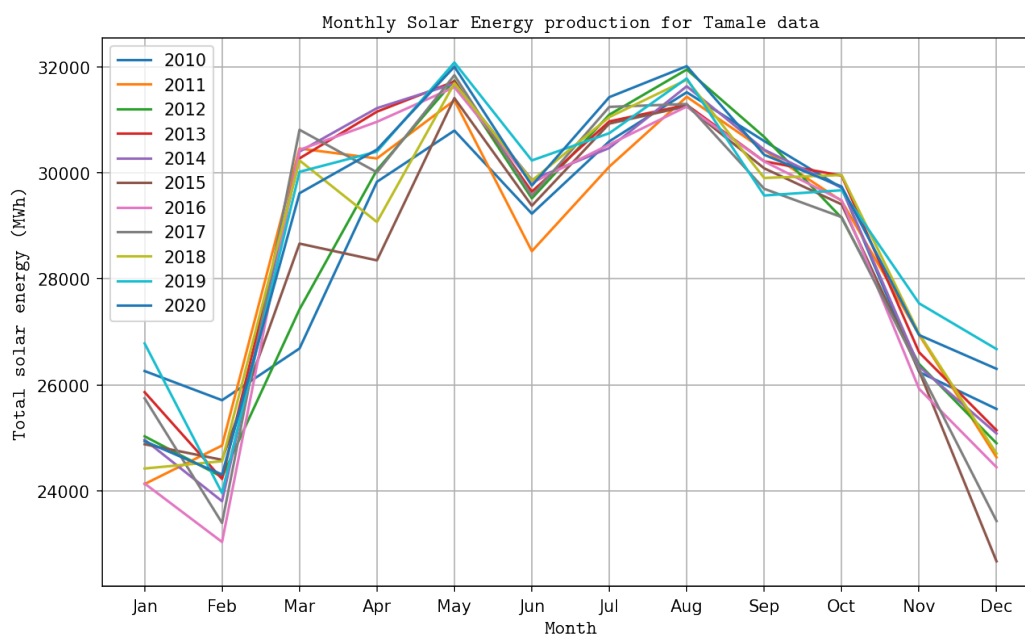


Figure 4: Cumulative monthly solar energy generation (Tamale).

3.3. Data Pre-processing

Time series forecasting is a predetermined sequence of observations, each recorded at a given time (Wu, Wang, Su, Tang and Wu (2020)). Time series data prediction, particularly in the solar energy industry, is highly difficult because

of the chaotic nature of the meteorological variables on which it is predicted. In addition, other challenges with time series data is determining which predictors are most useful for the time series label. Before using the feature engineering approach, the input variables are filtered and normalized.

After that we opted for automatic time series decomposition and Pearson correlation as data pre-processing approaches.

3.3.1. Automatic time series decomposition

ATSD deconstructs time series into seasonality, trend, and residual, which represent periodicity, long-term movements, and random variation, respectively. This paper looks at ways of using the ATSD to capture explicit periodicity in data to improve model accuracy. Upon realizing that there is seasonality and trend problem, the seasonal-decompose function, which conducts (ATSD) was imported. Similar to Dokumentov's seasonal-trend regression approach (Dokumentov and Hyndman (2022)) that allows for multiple and cyclic components, covariates, and seasonal patterns that have non-integer periods with complex topology. It is ideal for time series indexes such as hourly, daily, weekly, monthly, and quarterly data Oliveira, Francisco Filho, de Araújo, Celestino and Gomes (2020). The ATSD of multiple seasonal decompositions of a time series is presented below:

$$y_t = T_t + S_t + R_t \quad (3)$$

where the observed components in the series are denoted by y_t . Seasonal, trend and residual components are denoted by T_t , S_t , and R_t , respectively. The trend is the time series' growing and falling value, and the seasonal is the recurring short-term cycle. It represents the repetition of a specific pattern promptly after some periods. The residual, sometimes called the remainder, is the time series' random non-systematic fluctuation. Similar to mathematical operations, the residual is not exact; hence, an ATSD operation is needed. If the latent components are dependent on one another, the correlation is described in a multiplicative model as:

$$y_t = T_t * S_t * R_t \quad (4)$$

Trends, seasonality, and residual data were developed after examining the hourly, daily (24-H), and weekly (168-H) as potential effects on energy output. The form of the seasonal and trend components within each year is discovered to be dependent on the variable nature of the series. Certain aberrant maxima in the solar energy trend are documented for the weekly interval for the period studied. Furthermore, the residual fluctuations are due to changes affecting individual variables, causing the residual to swing in negative and positive directions. Upon realizing that these anomalies impact the model's performance, we set a lower limit by subtracting three times the residual standard deviation from the residual mean. Again, an upper limit threshold was created by multiplying the residual standard deviation by three, as illustrated in Figure 5. These procedures were used to eliminate anomalies from the residual data.

3.3.2. Pearson Correlation

Because the input variables have a multivariate probability distribution, Pearson correlation (Tastan (2019)) was utilized to discover which variables influence the other. This

correlation is frequently used when the variables are quantitative in nature, such as ratio or interval scale variables. Pearson's correlation coefficient is represented by r and is calculated as follows:

$$r = \frac{\sum (x_i - x_m) \sum (y_i - y_m)}{\sqrt{\sum (x_i - x_m)^2 \sum (y_i - y_m)^2}} \quad (5)$$

where the mean of x and y is represented by x_m and y_m . The value is always between -1 and 1. $r = -1$ or 1 shows that x and y have a perfect (positive or negative) correlation. $r = 0$ denotes that there is no or little correlation.

Initially, the correlation was performed on data without ATSD, and then on data with ATSD. As demonstrated in Figure 6, the connection of solar energy to the other variables with ATSD is better than without ATSD. In addition, we noticed that dampness had less of an impact on solar energy. Humidity, on the other hand, should not be overlooked because it has the potential to have a systemic impact. For example, the correlation of humidity to wind speed at 10 meters is -0.36, which is statistically significant. The analytical process is based on historical data and the most significant factors engineered utilizing ATSD. The ATSD is useful for smoothing the residual components' extremely positive and negative spikes. Pearson correlation was used to exclude irrelevant variables. This section goes through our suggested model, BDLSTM, and its advantages over MLP and the performance indicators we employed.

3.4. The Proposed Forecasting Methods

In a Jupiter notebook environment, the models are created utilizing Python modules such as Scikit-learn, Pandas, NumPy, SciPy, Matplotlib, and the TensorFlow framework. *Jupyter notebook was utilized because it is open-sourced all-in-one web-based interactive environment that combines the codes, rich text, images, mathematical equations and the graphical user interface in a single document during experiment.* A Train-Test-Val/split sample strategy was used to train the models. Out of the total of 96432 energy data, 80 per cent of the dataset representing 77146, was used for training, while the remaining 20 per cent representing 19286, was used for testing and validation. We started with the rectified linear unit (ReLU) activation function and then learned that tanh activation function aids in quick model learning, therefore tanh was picked as a time complexity trade-off. Dropout was used after each layer to reduce overfitting further and boost prediction capability. *Dropout at a rate of 0.1 is used at each layer, meaning one in five inputs will be randomly excluded from the update cycle, which regularizes the network to reduce overfitting.* Finally, we picked the ADAM optimizer (Achkar, Elias-Sleiman, Ezzidine and Haidar (2018)), which is computationally efficient, requires little memory to function and is appropriate for solving problems with noisy gradients. We employed 120 epochs and 256 batch sizes to reduce the error rate.

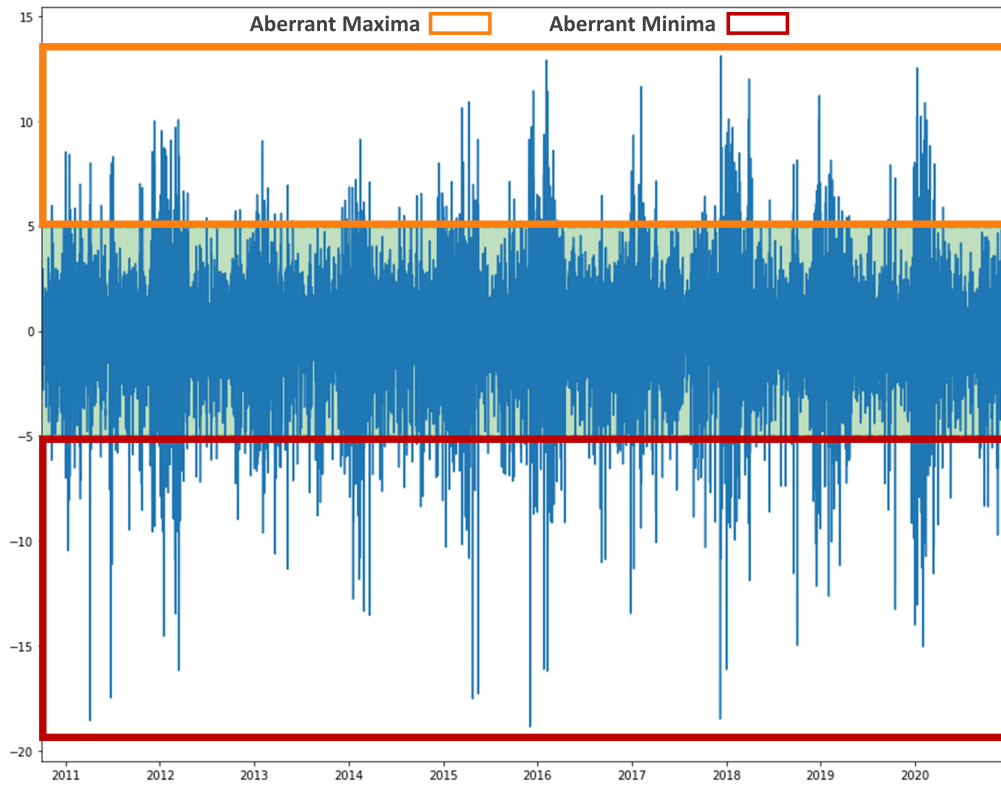


Figure 5: Weekly plots for decomposed residual threshold.

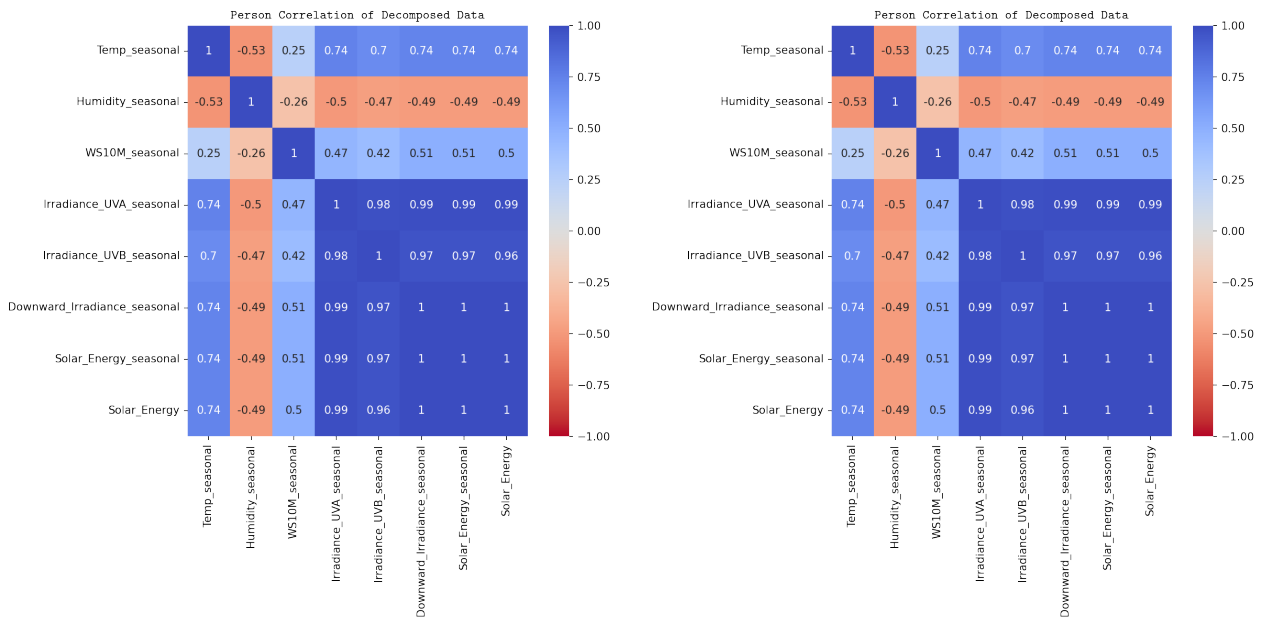


Figure 6: Pearson Correlation (a) without ATSD; (b) with ATSD

3.4.1. Multilayer Perceptron

The MLP is a prominent supervised learning model of the neural network used to assess solution functions, having numerous layers of neurons in its construction. *One major advantage of the multilayer perceptron is capable of*

learning any mapping functions and complex relationships, while single-layer perceptron only learns linear patterns. In most cases, MLP is trained using a direct technique based on a direct descent in stable conditions (Almonacid, Fernández, Mallick and Pérez-Higueras (2015)). Furthermore, the

response preparation of the feedback neural network (Honoria, Aguilera, Riesco and Zufiria (2001)), l is important in monitoring and assessing indirect plants and time-series forecasting models under changing conditions. There is, however the information travels in just one direction from the input layer to the output layer via linked channels (Gbémou, Eynard, Thil, Guillot and Grieu (2021)). *Due to the non-linearity of the data, the MLP was trained with two layers.* For an input layer $f(x) = x$, where x is an input vector and the network's hidden layers, $L = 1, \dots, l$ the following is given:

$$a^L(x) = b^L + W^L f^{L-1}(x) \quad (6)$$

$$f^L(x) = \phi(a^L(x)) \quad (7)$$

where b^L is the layer's bias vector L , W^L is the layer's weight matrix, and ϕ is the hidden neuron's activation function. Because we want to anticipate solar energy hourly, we set the timeframe to one hour. We tested the model with three thick layers, each with 100 neurons, 100 neurons, and one neuron.

3.4.2. Bi-directional LSTM

Traditional RNNs have a key drawback; they only use previous context states to predict future ones. Because they employ memory cells and gates to recall long-term dependencies in time series, LSTM networks are used as an alternative to RNNs. One significant limitation of traditional RNNs is that they only utilize prior context states to predict future states. LSTM networks are used as an alternative to RNNs because they use memory cells and gates to recall long-term dependencies in time series. *LSTM networks compute a hidden state h_t , which is the working memory of the LSTM as*

$$h_t = \tanh(c_t) * o_t \quad (8)$$

$$i_t = \sigma(x_t U^i + h_{t-1} W^i) \quad (9)$$

$$f_t = \sigma(x_t U^f + h_{t-1} W^f) \quad (10)$$

$$o_t = \sigma(x_t U^o + h_{t-1} W^o) \quad (11)$$

$$\bar{c}_t = \tanh(x_t U^g + h_{t-1} W^g) \quad (12)$$

$$c_t = \sigma(f_t * c_{t-1} + i_t * \bar{c}_t) \quad (13)$$

where the input, forget, and output is denoted by i_t, f_t , and o_t at time t , respectively. x_t and h_t are the number of

input components and hidden nodes, respectively. W and U are the weight matrices that are modified during training along the bias. The hidden state of the cell is represented by $c_t = \sigma$, while the unit's internal memory is represented by c_t . However, LSTM still has a drawback in that it only analyses the past context of the input and cannot evaluate any future context. To solve this constraint, BDLSTM was deployed by Aksoy, Ertürk, Erdogan, Eydurhan and Tariq (2018), which takes into account the data's past and future context, as shown in Figure 7. *Unlike the MLP, which is a feed-forward neural network, the BDLSTM has the following advantages:*

- *Allows the connection of the neural network to form a cycle, allowing information to persist.*
- *Capable of learning long-term dependencies by introducing the memory cell that replaces the artificial neurons in the network's hidden layers*
- *Deals with the challenge of vanishing and exploding gradients.*
- *With the memory cells, networks can associate memories, hence grasping the structure of the data dynamically over time prediction capacity.*

In addition, while the LSTM performs the same functions listed above, the BDLSTM have a superior function of processing information in both directions with two separate hidden layers, which is then propagated forward to the same output layer. The forward hidden layer h_t^f takes input in ascending order in the form $t=1,2,3,\dots, T$. The backward hidden layer h_t^b , adversely, evaluates the input in decreasing order in the form $t=T,\dots,3,2,1$. The following equations are used to implement the BDLSTM:

$$h_t^f = \tanh(x_t U_{xh}^f + h_{t-1}^f W_h^f) \quad (14)$$

$$h_t^b = \tanh(x_t U_{xh}^b + h_{t-1}^b W_h^b) \quad (15)$$

Finally, h_t^f and h_t^b are merged to produce y_t as follows

$$y_t = h_t^f + h_t^b \quad (16)$$

4. Experimental Results and Evaluation

4.1. Experimental Results

The validation of the proposed BDLSTM solar energy forecasting model's findings with decomposed data is shown in this section. To assess the results, several metrics are employed, including the Mean Absolute Error (*MAE*), Mean Square Error (*MSE*), Root Mean Square Error (*RMSE*), and R-squared. The following are their formulations:

$$MAE = 1/n \sum_{i=1}^n |y_i - y_{p_i}| \quad (17)$$

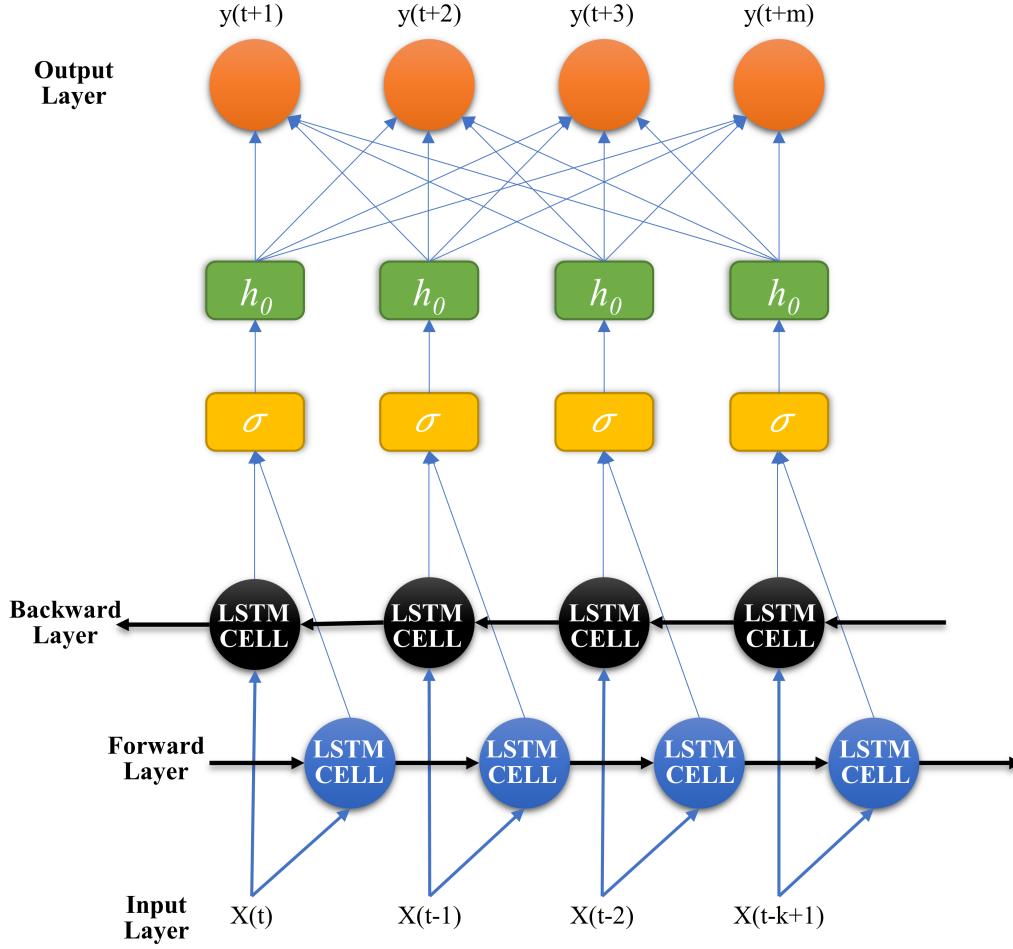


Figure 7: Illustration of Bi-directional LSTM.

$$MSE = 1/n \sum_{i=1}^n (y_i - yp_i)^2 \quad (18)$$

$$RMSE = \sqrt{1/n \sum_{i=1}^n (y_i - yp_i)^2} \quad (19)$$

$$R_{Squared} = (1 - ss_{regression})/ss_{total} \quad (20)$$

where y denotes the actual output, the yp_i denotes the forecasted output, and the n is the number of samples. The average of the absolute errors in Eq.(17) is used to compute *MAE*. Eq.(18) computes *MSE*, the difference between the true and the forecasted. When only minor mistakes are tolerated, Eq.(19) calculates *RMSE*, which is the square root of the *MSE*. Furthermore, to measure the forecasting accuracy of our models, we used *R-squared*, a statistical parameter in a regression model, to estimate the amount of

variation in the dependent variable that can be made explicit by the independent variable in Eq.(20), where $SS_{regression}$ is the sum of squares due to regression and SS_{total} is the total sum of squares. Also, the *R-squared* statistical parameter determines the amount of variation in the actual data that can be explained by the forecast value. Its significance is to show the goodness of fit for the regression model. Details of the metrics values based on the test data for the BDLSTM, other corresponding models, and ablation experiments by other papers are shown in Table 2. The findings are compared with the MLP model to demonstrate the consistency of the BDLSTM. The influence of ATSD is noticed in the consistency of Figure 8 and Figure 9 for decomposed data for both case study locations. The ability of BDLSTM to store and recognize information in both directions for extended time windows gives it an edge over MLP since learning for short time windows may not provide the best information on the data. *R-squared* values of 96.12 per cent, 99.90 per cent, and 99.91 per cent were found for the 1-hour, 24-hour, and 168-hour periods, respectively. On the ability to learn

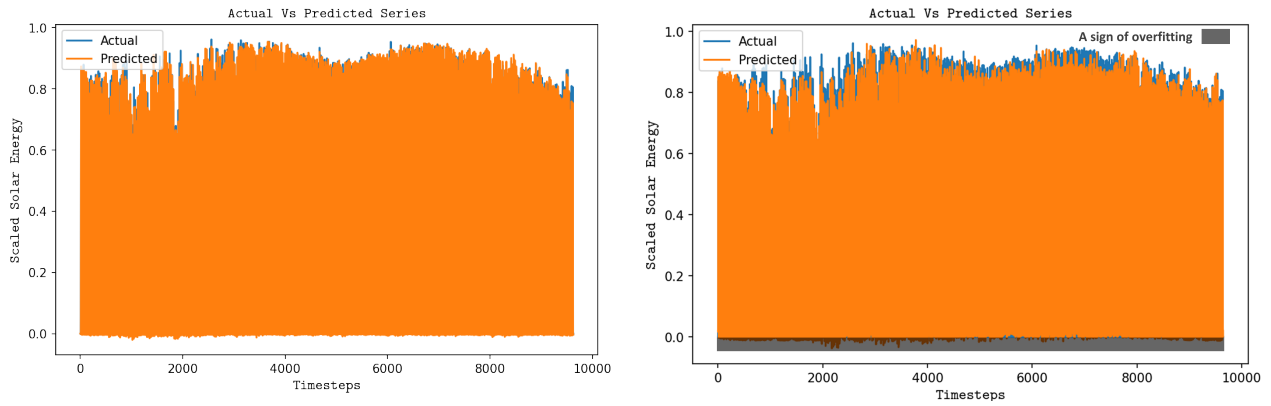


Figure 8: Actual and predicted values of solar energy related to Tamale (a) BDLSTM; (b) MLP

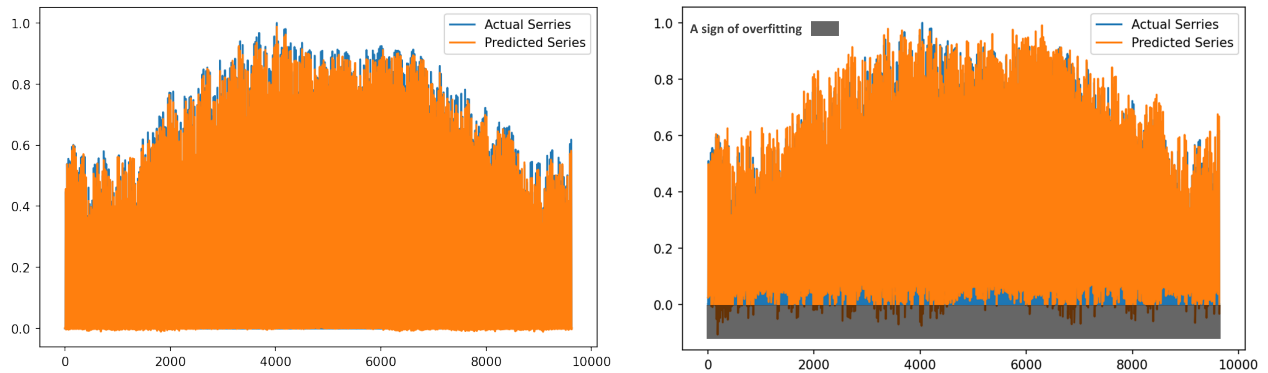


Figure 9: Actual and predicted solar energy values related to Wuhan (a) BDLSTM; (b) MLP

quickly, the learning computation time was dramatically decreased due to the compatibility of BDLSTM with the *tanh* activation function and the ADAM optimizer. Nonetheless, we notice that the MLP has the fastest training speed, at 2.15 seconds, compared to 6.95 seconds for the BDLSTM. It is important to note that using Google's GPU pro boosted training speed. Regardless, like all other deep learning models, the BDLSTM requires deep processing to train, which increases computational complexity, the BDLSTM remains a promising model for solar energy forecasting. Additionally, the curves for historical, actual, and predicted solar energy values shown in Figure 9 using the BLSTM, and the MLP, compared to Tamale's, the acquired data demonstrate the repeatability of our studied models. For the *RMSE*, the BDLSTM measures the best of 0.0093 compared to 0.0633 for MLP. We noted in Figure 12 (a) that, after using many dense layers, the *RMSE* value for the MLP is better at a 1-hour timescale than BDLSTM at the same timescale but it is also observed that the best performance of the BDLSTM at a 168-hour time window is because its bi-directional learning.

It is also worth noticing from Figure 11 that there is still an instance of overfitting with the MLP compared to the fitting BDLSTM. Overfitting happens when a model

learns the information and noise in the training data to the point that it adversely hampers its performance on validation data. This suggests that the MLP model does not detect but learns random fluctuations in the training data. The difficulty is that these concepts do not apply to validation data and negatively impact the models' ability to generalize compared to BDLSTM. Figure 12 presents the performance metrics graphs for solar energy prediction in Wuhan.

5. Conclusion and Future Work

This paper introduced the BDLSTM model for solar energy forecasting. The historical values for solar energy are estimated using the solar irradiance, values of the test bench PV module parameters, efficiency, and performance ratio to indicate a comprehensive implementation of the technique. A cloud-based server was embedded in the architecture for data storage, management and future predictions. A comparative analysis was then carried out on the performance of the BLSTM against LSTM and MLP. Because of its prominence in time series-based forecasting works, BDLSTM has become an algorithm of interest that the solar energy forecasting field benefits. Firstly, the models were experimented with data from Ghana's Northern Region, Tamale and secondly, with data from China's northern city,

Table 2
Performance comparison of metrics values based on the test data.

Models	Location	Timescales	MAE(MWH)	MSE(MWH)	RMSE(MWH)	R2 (%)
BDLSTM	Tamale, Ghana	168-H	0.0049	0.0001	0.0093	99.91
	Wuhan, China	168-H	0.0060	0.0001	0.0112	99.84
LSTM	Tamale, Ghana	168-H	0.0059	0.0001	0.0102	99.85
	Wuhan, China	168-H	0.0064	0.0001	0.0116	99.82
MLP	Tamale, Ghana	1-H	0.0358	0.0040	0.0633	96.30
	Wuhan, China	1-H	0.692	0.0076	0.0872	90.16
Other Researches						
Massaoudi et al. (2021) ERF	Australia	-	5.2100	-	8.3600	-
Claywell et al. (2020) ANFIS	Almeria, Spain	-	0.4222	-	0.5167	-
Claywell et al. (2020) MLP-GWO	Almeria, Spain	-	0.0773	-	0.1144	-
Hou et al. (2018) FOS-ELM	Dedougou, Bukina	-	0.5860	-	0.8310	97.9
Kim et al. (2019) RFR	South Korea	-	-	-	4.000	70.5

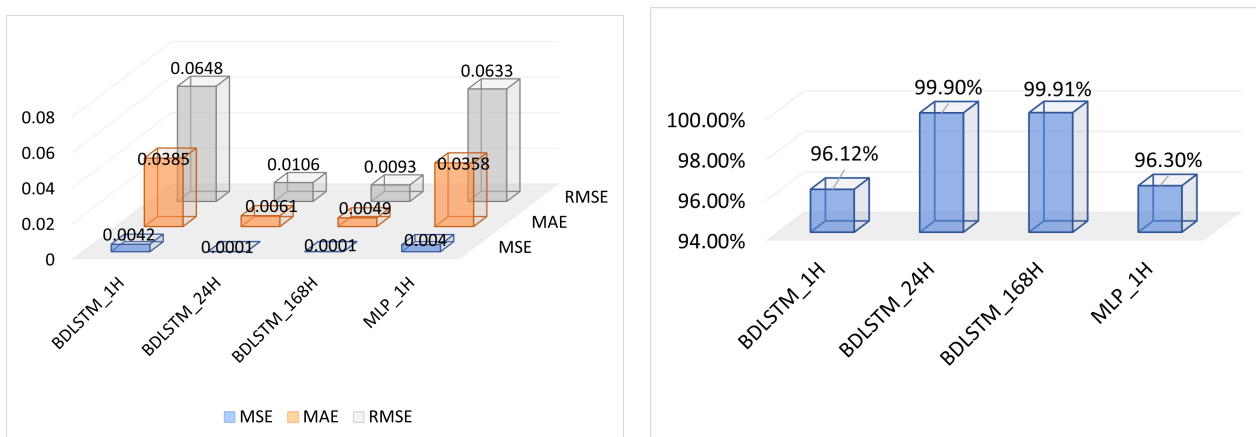


Figure 10: Performance metrics related to Tamale. (a) metric values; (b) R-squared values

Wuhan, to perform the hourly forecasting. The locations were chosen due to their parallel climatic variability. The outcomes were evaluated using four metrics: MSE, MAE, RMSE, and R-Squared, which examine prediction accuracy and error range. One limitation of forecasting research is the

unavailability of hardware components. Our future work will look at hosting a hardware cloud-based server for optimum data management.

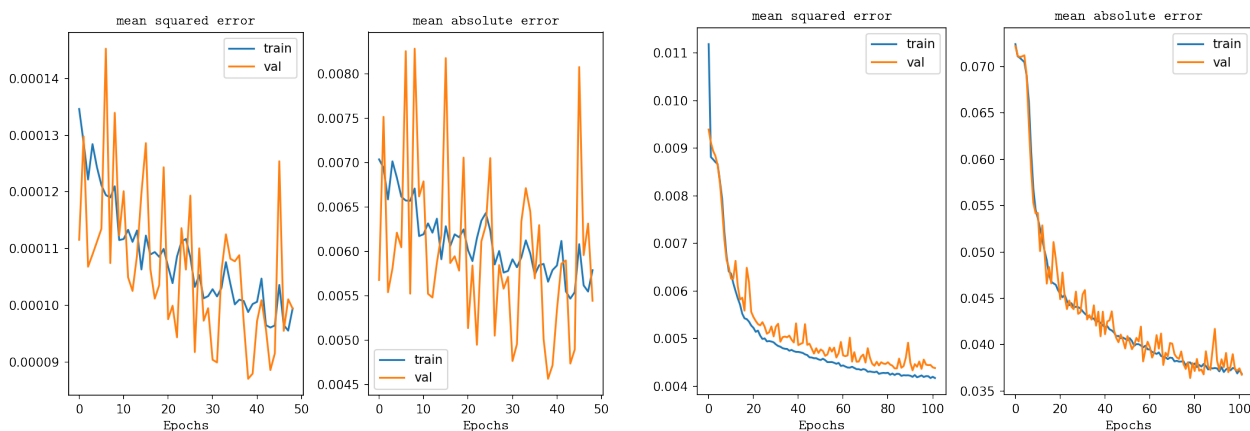


Figure 11: Training error rates and validation error rates (a) BDLSTM; (b) MLP

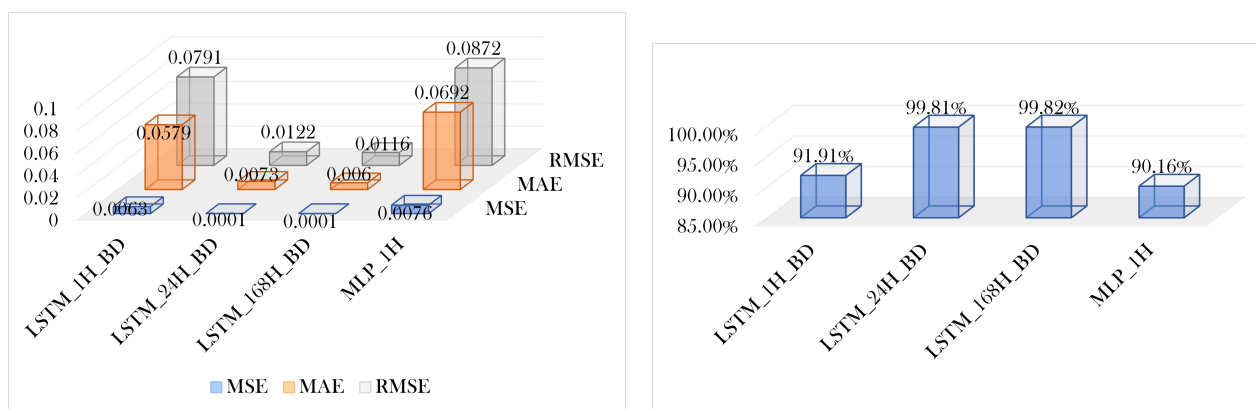


Figure 12: Performance metrics related to Wuhan (a) metric values; (b) R-squared

Acknowledgements

This work has received funding from the Key Laboratory Foundation of National Defence Technology under Grant 61424010208, National Natural Science Foundation of China (No. 41911530242 and 41975142), 5150 Spring Specialists (05492018012 and 05762018039), Major Program of the National Social Science Fund of China (Grant No. 17ZDA092), 333 High-Level Talent Cultivation Project of Jiangsu Province (BRA2018332), Royal Society of Edinburgh, UK and China Natural Science Foundation Council (RSE Reference: 62967_Liu_2018_2) under their Joint International Projects funding scheme and basic Research Programs (Natural Science Foundation) of Jiangsu Province, China (BK20191398 and BK20180794). Muhammad Attique was supported by National Research Foundation of Korea grant funded by the Korean Government (2020R1G1A1013221).

Author's Contributions

Qi Liu; Supervision, Visualization, Writing of original draft and editing. Oscar Famous Darteh; Conceptualization, Visualization, Writing of original draft and editing. Muhammad Bilal; Editing, Data Curation and investigation. Xianming Huang, Xiaodong Liu, Amevi Acakpovi; Investigation and formal analysis. Muhammad Attique; Editing and investigation.

Conflict of Interest

Authors declare no conflict of interest

References

- Abualigah, L., Zitar, R.A., Almotairi, K.H., Hussein, A.M., Abd Elaziz, M., Nikoo, M.R., Gandomi, A.H., 2022. Wind, solar, and photovoltaic renewable energy systems with and without energy storage optimization: a survey of advanced machine learning and deep learning techniques. *Energies* 15, 578. doi:10.3390/en15020578.
- Achkar, R., Elias-Sleiman, F., Ezzidine, H., Haidar, N., 2018. Comparison of bpa-mlp and lstm-rnn for stocks prediction, in: 2018 6th International Symposium on Computational and Business Intelligence (ISCBI), IEEE. pp. 48–51. doi:10.1109/ISCBI.2018.00019.
- Agada, I., Eweh, E., Aondoakaa, S., 2021. Time series arima model for predicting monthly net radiation. *FUDMA JOURNAL OF SCIENCES* 5, 182–193. doi:10.33003/fjs-2021-0504-805.
- Aksoy, A., Ertürk, Y.E., Erdogan, S., Eyduran, E., Tariq, M.M., 2018. Estimation of honey production in beekeeping enterprises from eastern part of turkey through some data mining algorithms. *Pakistan Journal of Zoology* 50, 2199–2207. doi:10.17582/journal.pjz/2018.50.6.2199.2207.
- Almonacid, F., Fernández, E., Mallick, T., Pérez-Higueras, P., 2015. High concentrator photovoltaic module simulation by neuronal networks using spectrally corrected direct normal irradiance and cell temperature. *Energy* 84, 336–343. doi:10.1016/j.energy.2015.02.105.
- AlSkaif, T., Dev, S., Visser, L., Hossari, M., van Sark, W., 2020. A systematic analysis of meteorological variables for pv output power estimation. *Renewable Energy* 153, 12–22. doi:10.1016/j.renene.2020.01.150.
- Bansal, N., Sharma, A., Singh, R., 2019. An evolving hybrid deep learning framework for legal document classification. *Ingénierie des Systèmes d'Information* 24. doi:10.18280/isi.240410.
- Benmouiza, K., Cheknane, A., 2016. Small-scale solar radiation forecasting using arma and nonlinear autoregressive neural network models. *Theoretical and Applied Climatology* 124, 945–958. doi:10.1007/s00704-015-1469-z.
- Cao, P., Yang, Z., Sun, L., Liang, Y., Yang, M.Q., Guan, R., 2019a. Image captioning with bidirectional semantic attention-based guiding of long short-term memory. *Neural Processing Letters* 50, 103–119. doi:10.1007/s11063-018-09973-5.
- Cao, Y., Yang, F., Tang, Q., Lu, X., 2019b. An attention enhanced bidirectional lstm for early forest fire smoke recognition. *IEEE Access* 7, 154732–154742. doi:10.1109/ACCESS.2019.2946712.
- Chen, B., Baek, S.W., Hou, Y., Aydin, E., De Bastiani, M., Scheffel, B., Proppe, A., Huang, Z., Wei, M., Wang, Y.K., et al., 2020. Enhanced optical path and electron diffusion length enable high-efficiency perovskite tandems. *Nature communications* 11, 1–9. doi:10.1038/s41467-020-15077-3.
- Cheng, Y., Zheng, Z., Wang, J., Yang, L., Wan, S., 2019. Attribute reduction based on genetic algorithm for the coevolution of meteorological data in the industrial internet of things. *Wireless communications and mobile computing* 2019, 1–9. doi:10.1186/s13638-019-1511-4.
- Choi, S., Hur, J., 2020. An ensemble learner-based bagging model using past output data for photovoltaic forecasting. *Energies* 13, 1438. doi:10.3390/en13061438.
- Claywell, R., Nadai, L., Felde, I., Ardabili, S., Mosavi, A., 2020. Adaptive neuro-fuzzy inference system and a multilayer perceptron model trained with grey wolf optimizer for predicting solar diffuse fraction. *Entropy* 22, 1192. doi:10.3390/e22111192.

- Cui, Z., Ke, R., Pu, Z., Wang, Y., 2020. Stacked bidirectional and unidirectional lstm recurrent neural network for forecasting network-wide traffic state with missing values. *Transportation Research Part C: Emerging Technologies* 118, 102674. doi:10.1016/j.trc.2020.102674.
- Darteh, O.F., Liu, Q., Oduro, C., Liu, X., Adjei, C.O., 2021. A survey on an artificial intelligence approach to maintenance of solar photovoltaic modules, in: *International Conference on Computational & Experimental Engineering and Sciences*, Springer. pp. 507–517. doi:10.1007/978-3-030-67090-0_41.
- Dokumentov, A., Hyndman, R.J., 2022. Str: Seasonal-trend decomposition using regression. *INFORMS Journal on Data Science* 1, 50–62.
- El Badaoui, H., Abdallaoui, A., Chabaa, S., 2013. Using mlp neural networks for predicting global solar radiation. *The International Journal Of Engineering And Science* 2, 48–56.
- Gbémou, S., Eynard, J., Thil, S., Guillot, E., Grieu, S., 2021. A comparative study of machine learning-based methods for global horizontal irradiance forecasting. *Energies* 14, 3192. doi:10.3390/en14113192.
- Harrou, F., Kadri, F., Sun, Y., 2020. Forecasting of photovoltaic solar power production using lstm approach. *Advanced statistical modeling, forecasting, and fault detection in renewable energy systems* 3. doi:10.5772/intechopen.91248.
- Hmamouche, Y., Przymus, P., Casali, A., Lakhal, L., 2017. Gfsm: a feature selection method for improving time series forecasting. *International Journal On Advances in Systems and Measurements* 10, 254–264. doi:https://hal.science/hal-02448277.
- Hontoria, L., Aguilera, J., Riesco, J., Zufiria, P., 2001. Recurrent neural supervised models for generating solar radiation synthetic series. *Journal of Intelligent and Robotic Systems* 31, 201–221. doi:10.1023/A:1012031827871.
- Hou, M., Zhang, T., Weng, F., Ali, M., Al-Ansari, N., Yaseen, Z.M., 2018. Global solar radiation prediction using hybrid online sequential extreme learning machine model. *Energies* 11, 3415. doi:10.3390/en11123415.
- Hu, Z., Xu, X., Zhang, Y., Tang, H., Cheng, Y., Qian, C., Khosravi, M.R., 2021. Cloud-edge cooperation for meteorological radar big data: a review of data quality control. *Complex & Intelligent Systems* , 1–15doi:10.1007/s40747-021-00581-w.
- Hunter, G.W., Vettorato, D., Sagoe, G., 2018. Creating smart energy cities for sustainability through project implementation: A case study of bolzano, italy. *Sustainability* 10, 21–67. doi:10.3390/su10072167.
- Ilunga, E.T., 2018. Short-term hourly load forecasting in south africa using neural networks. Ph.D. thesis. University of the Witwatersrand, Faculty of Science, School of Statistics.
- Jebli, I., Belouadha, F.Z., Kabbaj, M.I., Tilioua, A., 2021. Deep learning based models for solar energy prediction. *Advances Sci* 6, 349–355. doi:10.25046/aj060140.
- Jeong, Y., Yi, K., 2020. Bidirectional long shot-term memory-based interactive motion prediction of cut-in vehicles in urban environments. *IEEE Access* 8, 106183–106197. doi:10.1109/ACCESS.2020.2994929.
- Kim, K., Jeong, J., 2020. Real-time monitoring for hydraulic states based on convolutional bidirectional lstm with attention mechanism. *Sensors* 20, 7099. doi:10.3390/s20247099.
- Kim, S.G., Jung, J.Y., Sim, M.K., 2019. A two-step approach to solar power generation prediction based on weather data using machine learning. *Sustainability* 11, 1501. doi:10.3390/SU11051501.
- Li, G., Wang, H., Zhang, S., Xin, J., Liu, H., 2019. Recurrent neural networks based photovoltaic power forecasting approach. *Energies* 12, 2538. doi:10.3390/en12132538.
- Liu, Q., Kamoto, K.M., Liu, X., 2020a. Microgrids-as-a-service for rural electrification in sub-saharan africa. *Comput. Mater. Contin.* 63, 1249–1261. doi:10.32604/cmc.2020.05598.
- Liu, Q., Kamoto, K.M., Liu, X., Zhang, Y., Yang, Z., Khosravi, M.R., Xu, Y., Qi, L., 2020b. A sensory similarities approach to load disaggregation of charging stations in internet of electric vehicles. *IEEE Sensors Journal* 21, 15895–15903. doi:10.1109/JSEN.2020.3027684.
- Liu, Q., Nakoty, F.M., Wu, X., Anaadumba, R., Liu, X., Zhang, Y., Qi, L., 2020c. A secure edge monitoring approach to unsupervised energy disaggregation using mean shift algorithm in residential buildings. *Computer Communications* 162, 187–195. doi:10.1016/j.comcom.2020.08.024.
- Maciel, J.N., Ledesma, J.J.G., Junior, O.H.A., 2021. Forecasting solar power output generation: A systematic review with the prokno-c. *IEEE Latin America Transactions* 19, 612–624. doi:10.1109/TLA.2021.9448544.
- Massaoudi, M., Chihi, I., Sidhom, L., Trabelsi, M., Refaat, S.S., Oueslati, F.S., 2021. Enhanced random forest model for robust short-term photovoltaic power forecasting using weather measurements. *Energies* 14, 3992. doi:10.3390/en14133992.
- Matsumoto, T., Yamada, Y., 2021. Comprehensive and comparative analysis of gam-based pv power forecasting models using multidimensional tensor product splines against machine learning techniques. *Energies* 14, 7146. doi:https://doi.org/10.3390/en14217146.
- McCandless, T., Dettling, S., Haupt, S.E., 2020. Comparison of implicit vs. explicit regime identification in machine learning methods for solar irradiance prediction. *Energies* 13, 689. doi:https://doi.org/10.3390/en13030689.
- Minka, N.S., Ayo, J.O., et al., 2014. Influence of cold-dry (harmattan) season on colonic temperature and the development of pulmonary hypertension in broiler chickens, and the modulating effect of ascorbic acid. *Open Access Animal Physiology* 6. doi:10.2147/oaap.s51741.
- Mohanty, S., Patra, P.K., Sahoo, S.S., 2015. Prediction of global solar radiation using nonlinear auto regressive network with exogenous inputs (narx), in: *2015 39th National Systems Conference (NSC), IEEE*. pp. 1–6. doi:10.1109/NATSYS.2015.7489103.
- Na, Z., Wang, Y., Li, X., Xia, J., Liu, X., Xiong, M., Lu, W., 2018. Subcarrier allocation based simultaneous wireless information and power transfer algorithm in 5g cooperative ofdm communication systems. *Physical Communication* 29, 164–170. doi:10.1016/j.phycom.2021.101584.
- Oliveira, D.H., Francisco Filho, M., de Araújo, T.P., Celestino, J., Gomes, R.L., 2020. Adaptive model for network resources prediction in modern internet service providers, in: *2020 IEEE Symposium on Computers and Communications (ISCC), IEEE*. pp. 1–6. doi:10.1109/ISCC50000.2020.9219550.
- Pasion, C., Wagner, T., Koschnick, C., Schuldt, S., Williams, J., Hallinan, K., 2020. Machine learning modeling of horizontal photovoltaics using weather and location data. *Energies* 13, 2570. doi:10.3390/en13102570.
- POWER, N., 2018. Power data access viewer.
- Qing, X., Niu, Y., 2018. Hourly day-ahead solar irradiance prediction using weather forecasts by lstm. *Energy* 148, 461–468. doi:10.1016/j.energy.2018.01.177.
- Rajasegarar, S., Leckie, C., Palaniswami, M., Bezdek, J.C., 2007. Quarter sphere based distributed anomaly detection in wireless sensor networks, in: *2007 IEEE International Conference on Communications, IEEE*. pp. 3864–3869. doi:10.1109/ICCS1.2017.8326002.
- Ran, Z., Zheng, D., Lai, Y., Tian, L., 2020. Applying stack bidirectional lstm model to intrusion detection. *CMC-COMPUTERS MATERIALS & CONTINUA* 65, 309–320. doi:10.32604/cmc.2020.010102.
- Ritterbush, J., 2006. World weather information service. *Reference Reviews* .
- Saeed, A., Li, C., Danish, M., Saeed, R., Tang, G., Gan, Z., Ahmed, A., 2020. Hybrid bidirectional lstm model for short-term wind speed interval prediction. *IEEE Access* , 182283–182294doi:10.1109/ACCESS.2020.3027977.
- Shen, B., Xu, X., Qi, L., Zhang, X., Srivastava, G., 2021. Dynamic server placement in edge computing toward internet of vehicles. *Computer Communications* 178, 114–123. doi:10.1016/j.comcom.2021.07.021.
- Sindhu, S., Nehra, V., Luthra, S., 2017. Solar energy deployment for sustainable future of india: Hybrid swoc-ahp analysis. *Renewable and Sustainable Energy Reviews* 72, 1138–1151. doi:10.1016/j.rser.2016.10.033.
- Sola, Y., Lorente, J., 2015. Contribution of uva irradiance to the erythema and photoaging effects in solar and sunbed exposures. *Journal of Photochemistry and Photobiology B: Biology* 143, 5–11. doi:10.1016/j.jphotobiol.2014.10.024.
- Solar, S., Ag, T., 2016. Performance ratio-quality factor for the pv plant. *Sma* 1.

- Sun, S., Wang, S., Zhang, G., Zheng, J., 2018. A decomposition-clustering-ensemble learning approach for solar radiation forecasting. *Solar Energy* 163, 189–199. doi:10.1016/j.solener.2018.02.006.
- Swales, A., et al., 1999. Open modbus/tcp specification. *Schneider Electric* 29, 3–19.
- Tastan, H., 2019. Testing for spectral granger causality. *Stata J.* doi:10.1177/1536867x1501500411.
- Wang, Y., Liao, W., Chang, Y., 2018a. Gated recurrent unit network-based short-term photovoltaic forecasting. *Energies* 11, 2163. doi:10.3390/en11082163.
- Wang, Y., Shen, Y., Mao, S., Chen, X., Zou, H., 2018b. Lasso and lstm integrated temporal model for short-term solar intensity forecasting. *IEEE Internet of Things Journal* 6, 2933–2944. doi:10.1109/JIOT.2018.2877510.
- Wu, D., Wang, X., Su, J., Tang, B., Wu, S., 2020. A labeling method for financial time series prediction based on trends. *Entropy* 22, 1162. doi:10.3390/e22101162.
- Wu, H., Liu, Q., Liu, X., Zhang, Y., Yang, Z., 2022. An edge-assisted cloud framework using a residual concatenate fcn approach to beam correction in the internet of weather radars. *World Wide Web* , 1–27doi:10.1007/s11280-021-00988-y.
- Xu, X., Wang, S., Wang, Z., Zhang, X., Hu, R., 2021. Exploring image enhancement for salient object detection in low light images. *ACM Transactions on Multimedia Computing, Communications, and Applications (TOMM)* 17, 1–19. doi:10.1145/3401979.
- Yang, L., Li, Y., Wang, J., Tang, Z., 2019. Post text processing of chinese speech recognition based on bidirectional lstm networks and crf. *Electronics* 8, 12–48. doi:10.3390/electronics8111248.
- Ye, X., Chen, F., Hou, Z., 2015. Analysis on electric loads and temperature in wuhan city. *Procedia Engineering* 121, 2157–2162. doi:10.1016/j.proeng.2015.09.087.
- Zhang, J., Liu, Q., Chen, L., Tian, Y., Wang, J., 2021. Nonintrusive load management based on distributed edge and secure key agreement. *Wireless Communications and Mobile Computing* 2021. doi:10.1155/2021/6691348.
- Zhao, C., You, J., Wen, X., Li, X., 2020. Deep bi-lstm networks for sequential recommendation. *Entropy* 22, 870. doi:10.3390/E22080870.